ISSN (Print) 1226-1750
ISSN (Online) 2233-6656
Journal of Magnetics 30(4), 733-739 (2025) https://doi.org/10.4283/JMAG.2025.30.4.733

Analog Self-Synchronized Switching Technique for Stable High-Frequency Electromagnetic AC Stimulation in Neurorehabilitation

Sun-woo Lee[1], Seung min Hwang[2], Ji-young An[1], Young-Jin Jung[1,2]*, and In-suh Kim[3]*

[1]School of Biomedical Engineering, Chonnam National University, Yeosu 59626, Republic of Korea
[2]Department of Biomedical Engineering, Chonnam National University, Yeosu 59626, Republic of Korea
[3]Department of Physical Medicine and Rehabilitation, Inje University Busan Paik Hospital, Busan 47392, Republic of Korea

(Received 28 October 2025, Received in final form 11 December 2025, Accepted 15 December 2025)

Electromagnetic alternating current (AC) stimulation, a key application of applied electromagnetics, is a non-invasive neuromodulation technique that delivers low-intensity oscillating electric fields to the brain via scalp electrodes. Conventional microcontroller (MCU)-based devices face computational loads that compromise stability at high frequencies. We propose an analog self-synchronized switching algorithm where the MCU only controls the DAC, while an analog circuit autonomously manages switching. A system based on an ATmega328p (50 samples/cycle, n=10) was implemented to compare both methods. The proposed algorithm improved the maximum frequency by 62% (to 1,250 Hz). In the 500Hz-1.25kHz high-frequency band, the proposed method showed statistically superior SNR ($p < 0.002$). Notably, at 1.1 kHz, the SNR with the proposed method was 9.67 dB higher. The proposed method's mean SNR in this band was higher and significantly more stable (33.069 ±1.201 dB vs 25.406 ±2.886 dB). Our algorithm improves high-frequency stability and reduces MCU burden, providing a robust foundation for multi-channel systems. It is believed that the developed tool will make a meaningful contribution to the advancement of rehabilitation medicine and neuromodulation research.

Keywords : electromagnetic AC stimulation, analog synchronization, switching control, signal stability, microcontroller efficiency

1. Introduction

Electromagnetic alternating current (AC) stimulation is a non-invasive neuromodulation technique that delivers low-intensity oscillating electric fields to the brain via scalp electrodes. This method modulates neural activity by entraining brain oscillations or inducing synaptic plasticity [1], thereby altering cortical excitability [1-3]. Recently, AC stimulation has been applied as a therapy in various neuropsychiatric disorders, including chronic pain, insomnia, Alzheimer's disease, and depression. Reported outcomes include cognitive enhancement, improved motor performance, and increased attention [1, 4-8].

Conventional transcranial AC stimulation (tACS) primarily uses low frequencies (below 100 Hz), which presents several limitations [9, 10]. Scalp nerve endings are highly sensitive to low-frequency current, causing tingling or discomfort that limits the tolerable stimulation intensity [11]. Furthermore, the phosphene phenomenon, which causes a sensation of flashing light due to retinal effects, can degrade the quality of experiments when stimulating specific brain regions [12, 13].

To overcome these limitations, recent research has focused on high-frequency stimulation at ≥1 kHz. At high frequencies, skin impedance is lower and sensory nerve sensitivity is reduced, allowing stronger currents to be applied with less user discomfort [9]. However, conventional MCU-based digital control methods face fundamental limitations in reliably implementing such high-frequency stimulation with low-cost electric ICs. In a real-time control system, data acquisition, processing, and output updates must be completed within strict time windows; missing these deadlines degrades system stability [14]. When generating high-frequency signals, the interval between samples shortens to the microsecond

*Co-corresponding author: Tel: +82-61-659-7366
Fax: +82-61-659-7369, e-mail: yj@jnu.ac.kr
e-mail: insuh2427@icloud.com

(μs) scale, causing computational processing time shortages as the MCU must handle both waveform generation via DAC and analog switch control simultaneously [15]. Accumulated software-related delay factors, such as SPI communication latency, interrupting handling, and internal computations, create timing variability, which leads to signal-to-noise ratio (SNR) degradation and waveform distortion [16, 17].

Moreover, when expanding to multi-channel systems like Dual-tACS (such as temporal interference stimulation), independent waveform generation and phase control are required for each channel, increasing the MCU's computational load proportionally to the number of channels [18-19]. To solve this problem, this study proposes an **'analog self-synchronized switching'** technique that limits the MCU's role to waveform generation, while an analog circuit, based on the DAC output signal, autonomously handles the switching control. Using an ATmega328P MCU, we quantitatively analyze the superiority of the proposed method over the conventional digital control method in terms of switching frequency and signal-to-noise ratio (SNR), thereby establishing a design foundation for high-frequency and multi-channel electromagnetic AC stimulation systems.

2. Methods and Materials

This study compares the conventional approach (in which the MCU handles all control tasks) with the proposed approach (in which an analog circuit takes over the switching task). To this end, we implemented each structure and quantitatively analyzed them by measuring switching frequency and signal-to-noise ratio (SNR).

2.1. System Architecture and Implementation

Systems for both methods consist of an MCU (ATmega328P, Microchip, USA), DAC (DAC5311, TI, USA), and OP-AMPs (OPA4140, TI, USA), and operate with comparators (LM393, TI, USA), analog switches (DG412, Maxim Integrated, USA), and power supplies of ±15V and +3.3V.

2.1.1 Conventional Digital Control Method

In the conventional method, the MCU is responsible for both waveform generation and switching control. From a firmware perspective (Fig. 1A), the MCU first sequentially reads the sine wave values stored internally in order to generate the rectified waveform that controls the current source. It then determines the polarity (positive/negative) of each value. If negative, the value is converted to

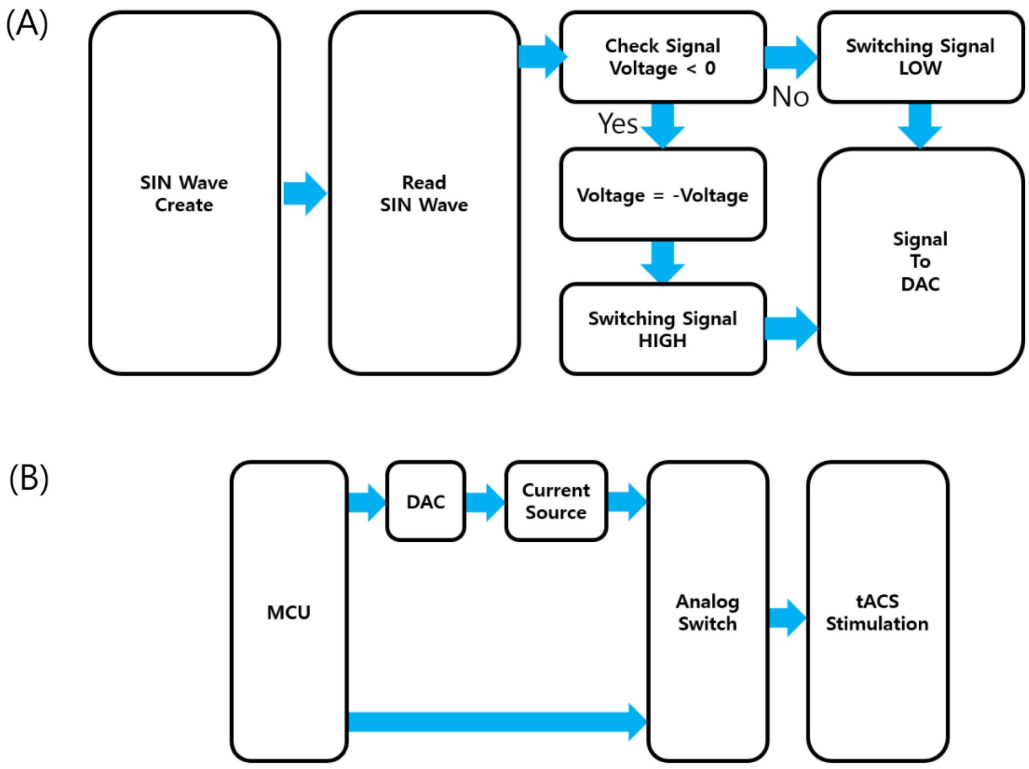

Fig. 1. (Color online) Conventional electromagnetic AC stimulator diagram. (A) Firmware that computes stimulation polarity and amplitude. (B) Hardware that applies the stimulation amplitude and direction according to the computed signal.

positive (rectified), and the switching signal is set to 'HIGH'; if positive, it is set to 'LOW'. This software logic is directly reflected in the hardware structure (Fig. 1B). In other words, the MCU simultaneously performs two roles: sending the rectified waveform to the DAC and controlling the analog switch and sending the polarity change timing signal to the analog switch. This structure, where all control is concentrated in the MCU's computation, can cause calculation delays and timing inaccuracies when generating high-frequency signals.

2.1.2. Proposed Analog Self-Synchronization Method

The proposed method focuses on drastically reducing the MCU's computational burden while increasing timing precision. From a firmware perspective (Fig. 2A), the MCU's role is highly simplified. Unlike in the conventional method, all software logic for polarity detection and switch control is eliminated; the MCU's sole task is now to sequentially read the internally stored sine-wave values and send them to the DAC. As the MCU's role is simplified, the remaining core functions are handled autonomously by the hardware (Fig. 2B). The DAC output, which receives the sine wave signal from the MCU, is split into two paths. The first path is connected to the comparator as a positive signal, detecting the phase of the DAC output signal in real-time to generate a synchronized switching signal that controls the analog switch. Simultaneously, the other path passes through a differential amplifier and a precision rectifier to become a waveform with a positive voltage, which is used as the signal to control the current source. By entrusting the switching control entirely to the hardware, software-related delay elements were fundamentally eliminated, securing the system's high-frequency stability.

2.2. Measurement Setup

Output waveforms were captured using an oscilloscope (MHO2024, Rigol, China). During measurement, the sampling rate was fixed at 100 KSa/s, and waveform data of 10-second length were collected for each condition. The collected data were saved as CSV files for subsequent analysis.

2.3. Experimental Procedure and Data Analysis

The experiment was conducted by implementing the circuits for each method. The final stimulation waveform was measured directly at the analog switch output terminal under conditions of 1 mA and 2 kΩ. First, both methods were set to 50 samples per sine wave cycle, and the maximum frequency that each system could stably generate was measured.

Next, the SNR of each method was measured at 8 frequency points from 500 Hz to 1.25 kHz to compare and analyze signal quality. To verify signal stability and

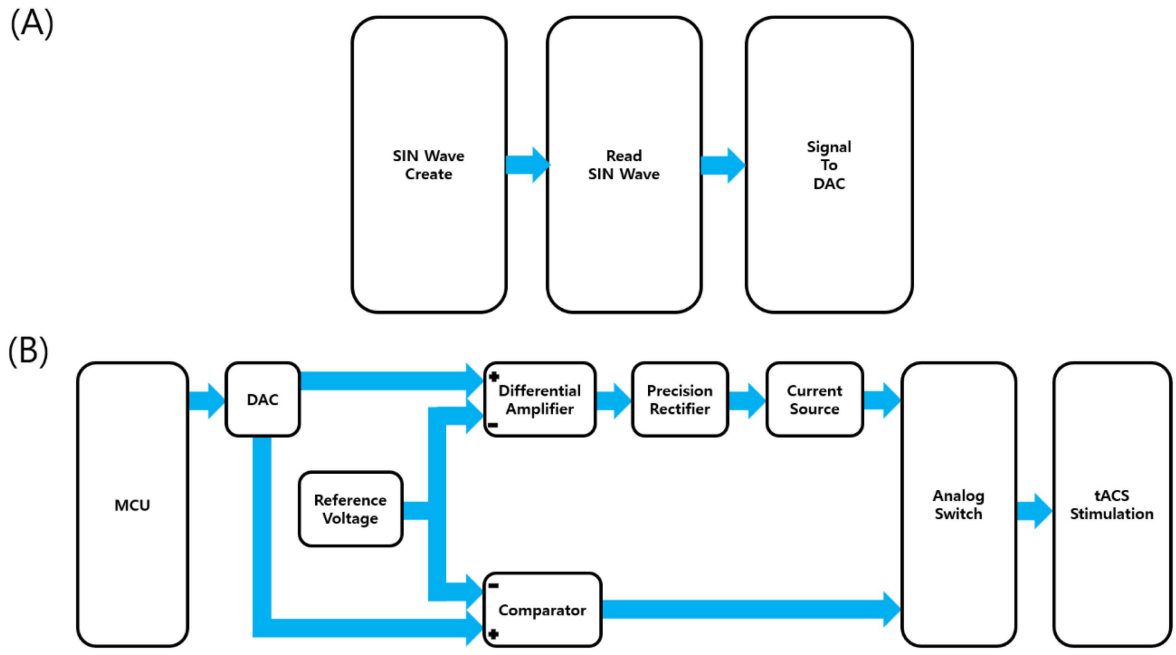

Fig. 2. (Color online) Proposed analog self-synchronized AC stimulator diagram. (A) Simplified firmware that generates only the sine-wave signal without performing switching control. (B) Hardware that autonomously determines switching timing and produces the stimulation signal using comparator and rectifier circuits.

statistical significance, waveform data were measured for 10 seconds under each frequency condition and then divided into 10 1-second epochs (n=10) to calculate the SNR for each epoch.

MATLAB (R2025a, MathWorks, USA) was used for data analysis. Fast Fourier Transform (FFT) was applied to the measured waveform data to analyze the frequency spectrum and determine the signal frequency from the highest peak in the frequency spectrum. SNR was calculated using MATLAB's built-in SNR function after extracting only the noise component by comparing the measured signal with an ideal sine wave signal of the same frequency.

For statistical analysis, the significance of the mean SNR difference between the two methods at each of the 8 frequency points was verified using a non-parametric paired comparison, the Wilcoxon signed-rank test. Furthermore, to compare the overall performance across the entire frequency band (500 Hz-1.25 kHz), the overall SNR mean and standard deviation for each method were calculated.

3. Results

This section first demonstrates the operating principle of the proposed analog self-synchronization method and then presents a quantitative comparison with the conventional digital control method in terms of switching speed and signal quality.

We verified that the proposed analog self-synchronization circuit operates as intended at each stage according to the design. Fig. 3 shows the time-domain waveforms measured at key points in the circuit. The initial sine wave (A) generated by the DAC passes through a differential amplifier and is precisely aligned to the 0V reference (B). Next, a precision rectifier produces the control signal (C) for the current source. Finally, the analog switch generates the phase-synchronized stimulation waveform (D), confirming the proper operation of the final stage. This result visually demonstrates that each component of the proposed system is operating seamlessly.

The improvement in timing stability was qualitatively confirmed by capturing and directly comparing the final output waveforms of the two methods under 1 mA, 2 KΩ

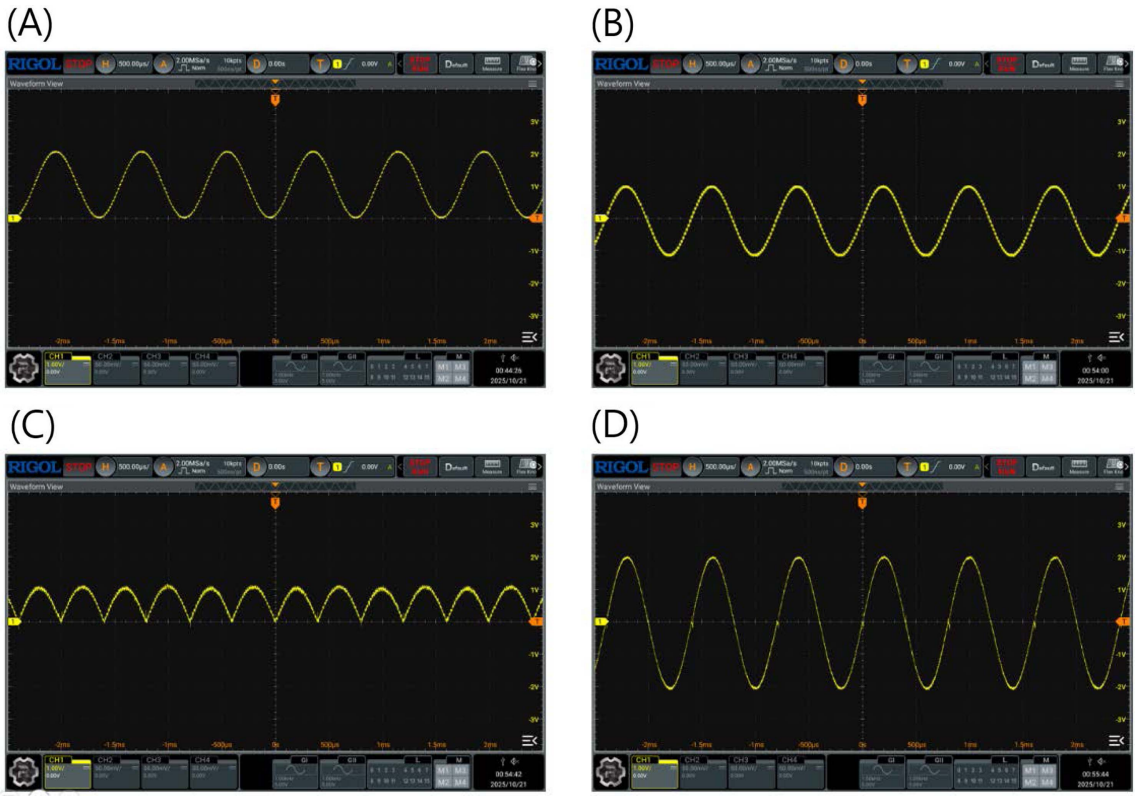

Fig. 3. (Color online) Verification of the proposed analog self-synchronized switching mechanism through oscilloscope measurements at key circuit nodes. (A) Original sine wave generated at the DAC output by the MCU. (B) Differential amplifier output aligned precisely to the 0 V reference. (C) Rectified control signal used to drive the current source. (D) Final stimulation waveform produced through the current source under load conditions (1mA, 2KΩ).

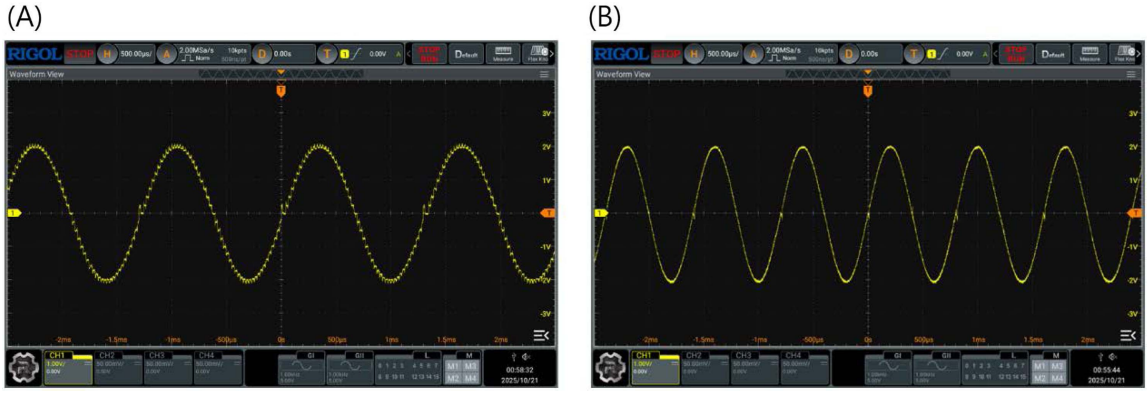

Fig. 4. (Color online) Comparison of final output waveforms (1 mA, 2 KΩ) (A) Switching signals of existing electromagnetic alternating current stimulators (B) Switching signals of devices with proposed self-synchronization algorithms in the same number of sinusoidal samples.

Table 1. Maximum Output Frequency Comparison in Same Number of Samples (50/Period) Conditions. The proposed method achieves 1,250 Hz, a 62% improvement over the conventional MCU-based method.

Condition	Frequency (Hz)
Conventional method	770 Hz
Proposed method	1250 Hz

conditions. As seen in Fig. 4, the waveform of the conventional method (A) exhibits a relatively noticeable "staircase" phenomenon, with minute temporal irregularities observed at the peaks and zero-crossing points of the waveform. In contrast, the waveform of the proposed method (B) shows a smoother shape and an overall uniform and stable waveform. This indicates that timing precision was improved as the switching control was performed at the hardware level.

First, the maximum frequency that each system could stably generate was measured under the condition of an identical number of sine wave samples (50 samples/period). As shown in Table 1, the conventional method achieved a maximum of 770 Hz, whereas the proposed method achieved 1,250 Hz, demonstrating a switching frequency improvement of about 62%. This implies that the MCU's computational burden was reduced, allowing data to be transmitted to the DAC at a faster speed.

Figure 5 and Table II show the mean and standard deviation of the SNR measured 10 times (n=10) at 8 frequency points from 500 Hz to 1.25 kHz. The Wilcoxon signed-rank test results showed that the SNR difference between the two methods was statistically highly significant at all frequency points from 500 Hz to 1.25 kHz ($p < 0.002$).

The superiority of the proposed method was clearly evident across the entire measured high-frequency band (500 Hz to 1.25 kHz). The proposed method maintained a stable SNR of over 30dB in the entire 500 Hz to 1.25 kHz

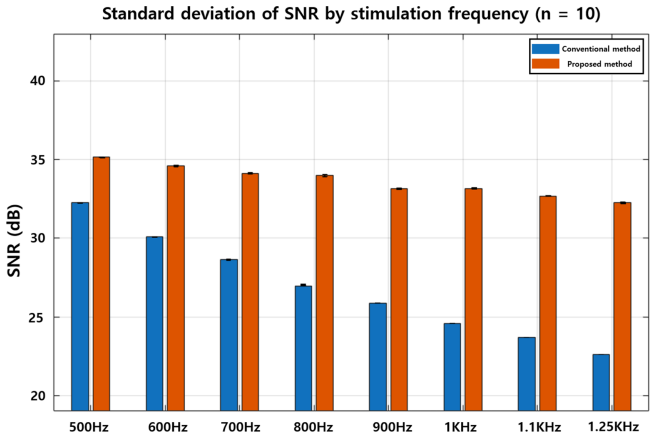

Fig. 5. (Color online) SNR standard deviation by frequency (SD, n = 10, 1 second interval).

Table 2. SNR results between conventional methods and self-synchronization control algorithms up to 500 Hz-1250 Hz. The proposed method maintains significantly higher SNR across all frequencies ($p < 0.002$).

Frequency (Hz)	Conventional method (n=10)	Proposed method (n=10)
500	30.09 (±0.06) dB	34.60 (±0.12) dB
600	28.66 (±0.02) dB	34.12 (±0.08) dB
700	26.97 (±0.03) dB	33.99 (±0.17) dB
800	25.88 (±0.02) dB	33.15 (±0.10) dB
900	24.58 (±0.02) dB	33.16 (±0.05) dB
1,000	23.15 (±0.58) dB	32.68 (±0.08) dB
1,100	22.60 (±0.04) dB	32.27 (±0.08) dB
1,250	21.32 (±0.02) dB	30.58 (±0.11) dB

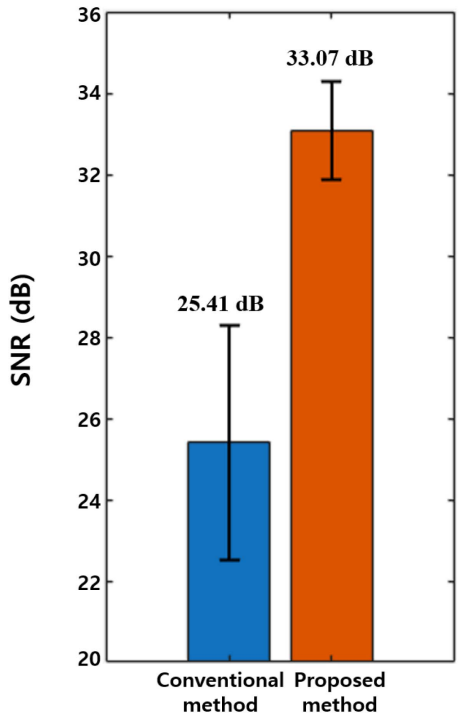

Fig. 6. (Color online) Comparison of mean SNR (± SD) across the entire frequency band for the conventional and proposed methods (n=10). A statistically significant difference between the two groups was observed, with a *p*-value less than 0.01.

range, whereas the SNR of the conventional method dropped sharply as the frequency increased. Notably, at 1.1 kHz, when the conventional method's SNR dropped to 22.60 ± 0.04 dB, the proposed method maintained 32.27 ±0.08 dB, showing a large difference of about 9.67 dB. Even at the maximum frequency of 1.25 kHz, the proposed method (30.58 ± 0.11 dB) recorded an SNR about 9.26 dB higher than the conventional method (21.32 ± 0.02 dB).

Figure 6 and Table III summarize the overall mean and standard deviation of the SNR across the high-frequency band (500 Hz-1.25 kHz). The overall mean SNR of the conventional method was 25.406 ± 2.886 dB, while the proposed method was measured at 33.069 ± 1.201 dB. This suggests not only that the proposed method provides higher signal quality overall, but also that its standard deviation (SD) is remarkably lower (1.201 dB) compared to the conventional method (2.886 dB), indicating far less performance variability across frequencies and greater stability. These results demonstrate that the proposed method has excellent performance in effectively suppressing signal distortion and noise generated during high-frequency stimulation, and that signal quality is maintained at high frequencies.

Table 3. Summary of overall mean SNR (± SD) for conventional and proposed methods (n=10). The proposed method shows higher signal quality (33.07 ± 1.20 dB) and lower variability than the conventional method (25.41 ± 2.89 dB).

Parameter	Conventional method (n=10)	Proposed method (n=10)
MEAN ± SD	25.406 dB (±2.886) dB	33.069 dB (±1.201) dB

4. Discussion

Experimental results indicate that the proposed method achieved a notable improvement in switching frequency. In terms of signal-to-noise ratio (SNR), it significantly outperformed the conventional approach in the 500 Hz to 1.25 kHz high-frequency range, demonstrating enhanced stability. These findings suggest that the hardware offloading strategy is an effective solution for mitigating timing instability and computation-induced jitter in microcontroller unit (MCU)-based neuromodulation systems.

The observed performance differences in the high-frequency band are attributed to each method's control characteristics. In the conventional method, as frequency increases, the sampling interval shortens, and timing variability due to the MCU's computation and communication delays escalates, leading to significant SNR degradation. In contrast, by delegating switching control to dedicated hardware, the proposed method maintains stable timing, yielding a 9.67 dB SNR advantage at 1.1 kHz. Additionally, the overall standard deviation of SNR in the proposed method (1.201 dB) was markedly lower than that of the conventional method (2.886 dB), indicating consistent signal quality across the tested high-frequency band.

While the system showed excellent high-frequency performance, limitations were also observed. Minor distortions due to the non-ideal behavior of analog switches, such as high on-resistance and leakage currents, were evident during zero-crossing transitions. These could lead to issues like simultaneous conduction, suggesting the need for further circuit optimization.

Despite these challenges, the proposed method offers a practical hardware architecture capable of supporting stable high-frequency stimulation, particularly beneficial in multi-channel systems. By relieving the MCU from switching control duties, more resources can be allocated to waveform generation and per-channel operations. This enables robust implementation of complex stimulation paradigms such as Dual-AC and high-density stimulation arrays, ultimately contributing to the advancement of non-

invasive neuromodulation technologies.

Moreover, this hardware foundation is highly compatible with Temporal Interference Stimulation (TIS)—a novel technique enabling non-invasive, spatially precise modulation of deep brain structures using the interference of multiple high-frequency currents [20, 21]. TIS has demonstrated the ability to stimulate deep neural targets, such as the hippocampus or subthalamic nucleus, without significantly affecting superficial tissues, thus overcoming the depth–focality trade-off of conventional transcranial stimulation [22, 23]. Importantly, TIS operates via standard scalp electrodes and simple signal generators, offering a low-cost and hardware-efficient platform for deep brain modulation [24, 25]. Such characteristics make it a promising candidate for use in multi-channel systems and portable therapeutic devices.

Recent studies have highlighted the clinical potential of TIS in neurological rehabilitation and disease treatment. Applications range from the suppression of epileptic activity [22], enhancement of motor performance [25], to modulation of deep nuclei involved in movement disorders like Parkinson's disease [23]. These advances underscore that the integration of stable, hardware-efficient architectures with techniques like TIS can facilitate the development of scalable, non-invasive neuromodulation tools for both clinical and research settings. It is anticipated that this work will contribute meaningfully to the progress of next-generation brain stimulation technologies for rehabilitation medicine and therapeutic brain modulation.

Acknowledgment

This result was supported by the "Regional Innovation System & Education (RISE)" through the Gwangju RISE Center, funded by the Ministry of Education (MOE) and the Gwangju Metropolitan Government, Republic of Korea (2025-RISE-05-011) & the Bio & Medical Technology Development Program of the National Research Foundation (NRF) funded by the Korean government (MSIT) (2021M3A9E4081781).

References

[1] Z. Zhao, S. Shirinpour, H. Tran, M. Wischnewski, and A. Opitz, J. Neural Eng. **21**, 026024 (2024).
[2] B. Asamoah, A. Khatoun, and M. Laughlin, Nat. Commun. **10**, 266 (2019).
[3] O. Elyamany, J. Iffland, J. Bak, C. Classen, G. Nolte, T. Schneider, G. Leicht, and C. Mulert, Brain Stimul. **18**, 780 (2025).
[4] D. Agboada, Z. Zhao, and M. Wischnewski, Front. Hum. Neurosci. **19**, 1548478 (2025).
[5] D. Serrano-Muoz, J. Avendao-Coy, C. Simon-Martinez, J. Taylor, and J. Gmez-Soriano, J. Neuroeng. Rehabil. **17**, 22 (2020).
[6] I. Alekseichuk, M. Wischnewski, and A. Opitz, Brain Stimul. **15**, 1222 (2022).
[7] A. Guerra, A. Suppa, M. Bologna, V. D'Onofrio, E. Bianchini, P. Brown, V. Lazzaro, and A. Berardelli, Brain Stimul. **11**, 734 (2018).
[8] N. Nissim, D. McAfee, S. Edwards, A. Prato, J. Lin, Z. Lu, H. Coslett, and R. Hamilton, Neuromodulation **26**, 728 (2023).
[9] C. S. Herrmann, S. Rach, T. Neuling, and D. Strber, Front. Hum. Neurosci. **7**, 279 (2013).
[10] L. Chaieb, A. Antal, and W. Paulus, Restor. Neurol. Neurosci. **29**, 167 (2011).
[11] G. Hsu, F. Farahani, and L. C. Parra, Brain Stimul. **14**, 693 (2021).
[12] D. J. Schutter and R. Hortensius, Clin. Neurophysiol. **121**, 1080 (2010).
[13] K. Kar and B. Krekelberg, J. Neurophysiol. **108**, 2173 (2012).
[14] P. G. Paulin, C. Liem, M. Cornero, F. Nacabal, and G. Goossens, Proc. IEEE **85**, 419 (1997).
[15] S. D. Adams, K. E. Bennet, S. J. Tye, M. Berk, and A. Z. Kouzani, PLoS ONE **14**, e0212554 (2019).
[16] S. Y. Chang, C. J. Kimble, I. Kim, S. B. Paek, K. R. Kressin, J. B. Boesche, S. V. Whitlock, D. R. Eaker, A. Kasasbeh, A. E. Horne, C. D. Blaha, K. E. Bennet, and K. H. Lee, J. Neurosurg. **119**, 1556 (2013).
[17] J. Erkens, M. Schulte, M. Vormann, A. Wilsch, and C. S. Herrmann, Neurosci. Insights **16**, 2633105520988854 (2021).
[18] L. Wu, T. Liu, and J. Wang, Front. Hum. Neurosci. **15**, 652393 (2021).
[19] Z. Zhu, Y. Xiong, Y. Chen, Y. Jiang, Z. Qian, J. Lu, Y. Liu, and J. Zhuang, Neural Plast. **2022**, 7605046 (2022).
[20] N. Grossman, D. Bono, N. Dedic, S. B. Kodandaramaiah, A. Rudenko, H.-J. Suk, A. M. Cassara, E. Neufeld, N. Kuster, L. H. Tsai, and E. S. Boyden, Cell **169**, 1029.e16 (2017).
[21] R. Liu, G. Zhu, Z. Wu, Y. Gan, J. Zhang, J. Liu, and L. Wang, Neuroimage **291**, 120581 (2024).
[22] E. Acerbo, A. Jegou, C. Luff, S. B. Kodandaramaiah, E. D. Glowacki, A. S. Dickey, and A. Williamson, Front. Neurosci. **16**, 945221 (2022).
[23] M. Lamoš, M. Bočková, F. Missey, C. Lubrano, M. De Araujo E Silva, J. Trajlinek, O. Studnicka, P. Daniel, R. Carron, V. Jirsa, J. Chrastina, R. Jančálek, E. D. Glowacki, A. Cassara, E. Neufeld, I. Rektorová, and A. Williamson, Mov. Disord. **40**, 1051 (2025).
[24] C. E. Luff, P. Dzialecka, E. Acerbo, A. Williamson, and N. Grossman, Brain Stimul. **17**, 92 (2024).
[25] S. Zheng, T. Fu, J. Yan, Y. Wang, Q. Li, H. Hu, J. Su, G. Chen, and P. Wang, J. Neuroeng. Rehabil. **21**, 38 (2024).